

Measurements of residual stresses in Al film/silicon nitride substrate microcantilever beam systems

Chiao-Chi Lin

Department of Materials Science and Engineering, National Tsing Hua University, Hsinchu 30013, Taiwan

Weileun Fang

Department of Power Mechanical Engineering, National Tsing Hua University, Hsinchu 30013, Taiwan

Hung-Yi Lin

Mechanical and System Research Laboratories, Industrial Technology Research Institute, Chutung, Hsinchu 31040, Taiwan

Chun-Hway Hsueh

Department of Materials Science and Engineering, National Taiwan University, Taipei 10619 Taiwan

Sanboh Lee^{a)}

Department of Materials Science and Engineering, National Tsing Hua University, Hsinchu 30013, Taiwan

(Received 25 November 2010; accepted 28 March 2011)

Microcantilevers fabricated by microelectromechanical system processes were used to study the residual stresses in the film/substrate systems. Aluminum films were deposited on silicon nitride substrates by thermal evaporation at room and elevated temperatures, and residual stresses were characterized from the deflection profiles of the Al/SiN_x microcantilevers. The Al/SiN_x microcantilever beam made of room-temperature-deposited Al film was found to deflect toward the substrate side, which in turn resulted in compressive residual stress in the film. In contrary, the microcantilever of Al film deposited at 105 °C was found to deflect toward the side of Al film when the thickness ratio of film to substrate was greater than 0.31 and the residual film stresses were tensile. The axes with zero bending strain component and zero stresses, i.e., the bending and the neutral axes in the film/substrate system were also investigated. The results can be applied to the arm of the atomic force microscope to characterize its deflection and stresses.

I. INTRODUCTION

The functionality and reliability of film/substrate systems are strongly influenced by residual stresses. These residual stresses can result from many sources, such as the thermal mismatch between the film and substrate,^{1–3} defects in the films (grain boundaries, dislocations, voids, and impurities) during the film deposition process,^{4–6} lattice mismatch between two single crystal materials,⁷ and the surface stress in the film.⁸ The residual stresses in the film/substrate systems also depend on the materials properties of the constituents and the film deposition process. For example, the residual stresses of the sputtered Al films depend not only on the film thickness but also on the sputtering pressure, substrate bias, and substrate materials.^{9–11} Different residual stresses may influence the film growth mode and the adatom mobility during different processing stages. Therefore, several theoretical models have been developed to

analyze the residual stresses in the film/substrate systems using the mechanical equilibrium conditions.^{1,12–14}

Various techniques have been developed to measure the residual stresses of the film/substrate system.^{15–22} Among those techniques, the approach of microcantilever beam has been widely used.^{2,3,19–22} Furthermore, due to the superior mechanical properties and the convenience of integrating in microelectromechanical system processes,²³ silicon nitride is a candidate to produce flexible microcantilever with a sharp tip for atomic force microscope (AFM).^{24–27} Gold or aluminum layer was generally deposited to increase the reflectivity of the silicon nitride microcantilevers.^{26,27} However, the residual stresses in the Al (or Au) and silicon nitride systems will inevitably influence the mechanical properties and reliabilities of the microcantilever systems. Hence, it prompted us to investigate the residual stresses in Al film deposited on silicon nitride at two deposition temperatures using the technique of microcantilever.

II. EXPERIMENTAL

The schematic drawing of the processes to fabricate microcantilevers is shown in Fig. 1. Double-side polished

^{a)}Address all correspondence to this author.
e-mail: sblee@mx.nthu.edu.tw
DOI: 10.1557/jmr.2011.111

4" Si wafers (Summit-Tech Resource Corp., Hsinchu, Taiwan) with (100) orientation and 550- μm thickness were used to carry out the conventional bulk micromachining. As shown in Fig. 1(a), silicon nitride (Si_xN_y) film with 940 ± 28 nm thickness was firstly deposited on both sides of the wafer by low-pressure chemical vapor deposition (LPCVD; 400104-FUR, TYSTAR Corporation, Torrance, CA) with the reaction gas of 24 sccm dichlorosilane and 6.9 sccm ammonia. The deposition temperature and pressure were 875 °C and 0.1 Torr, respectively. Patterns of predetermined microcantilever beams with 100- μm length and 10- μm width were formed by lithography on one side of the Si_xN_y coated wafer. After pattern transferred by dry etching and removal of the photoresists on the wafer [see Fig. 1(b)], wet etching with 45% (weight) KOH solution at 30 °C was used to remove the silicon underneath the Si_xN_y microcantilevers as shown in Fig. 1(c). The samples with Si_xN_y microcantilevers were finally rinsed by distilled water and then baked. The measurements of the thickness and the profile of microcantilevers were carried out by AFM (Dimension 3100; Digital Instrument Inc., Tonawanda, NY) and scanning electron microscope (SEM; JSM-6500F, JEOL Ltd., Tokyo, Japan). Elemental analyses of Si_xN_y were performed by energy dispersive x-ray (EDX) spectroscopy using the JSM-6500F SEM with a Si/Li EDX detector. Finally, the Al film was deposited on the Si_xN_y microcantilever as shown in Fig. 1(d).

The deflections of microcantilevers were measured by WYKO interferometer (Veeco Instruments, Plainview,

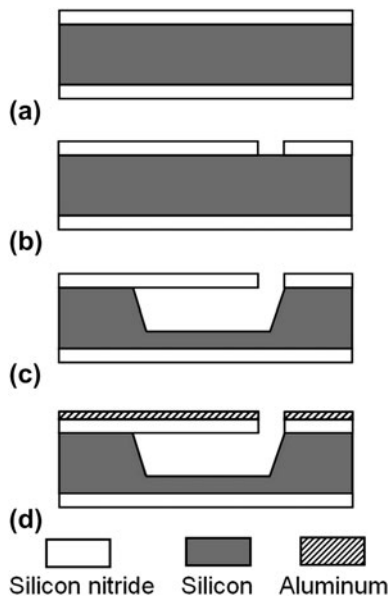


FIG. 1. Schematic of the fabrication process for microcantilever: (a) Si_xN_y deposition on double-side polished 4" Si wafer; (b) In-plane shape of the microcantilever defined and patterned on the Si_xN_y film using the photolithography and dry etching processes; (c) KOH wet etching to remove the silicon underneath the Si_xN_y microcantilever; and (d) Al evaporation on the Si_xN_y microcantilever.

NY) before and after the deposition of Al films. The WYKO measurement was carried out at room temperature and at least five microcantilevers were measured per sampling interval. For Al film deposition, thermal evaporation with Al source (99.99% purity) was performed with the pressure of 5×10^{-6} Torr at 25 and 105 °C, respectively. The deposition temperature was controlled by the substrate water-cooling system and quartz heating lamp. The thickness and surface morphology of Al films were measured by AFM. From the deflection data, the residual stresses in the Si_xN_y substrate and Al film were analyzed.

III. RESULTS AND DISCUSSION

The profiles of microcantilevers were measured before and after Al deposition. Figure 2 shows the typical profile of an uncoated Si_xN_y microcantilever measured by WYKO, where the radius of curvature of the uncoated Si_xN_y microcantilever is 1313.7 ± 39.4 μm . The curvature of the uncoated Si_xN_y microcantilever is due to the gradients of Si/N ratio and the atomic density in the direction of thickness.^{28–30} EDX analysis of Si_xN_y shows a nonfixed ratio of x to y, which indicates that the LPCVD silicon nitride herein is nonstoichiometric, i.e., SiN_x .³¹ For coated microcantilevers, the radius of curvature and surface roughness of microcantilevers as functions of Al film thickness are shown in Figs. 3(a) and 3(b), respectively. For the room-temperature-deposited microcantilevers, the radius of curvature decreases with increasing film thickness. However, for 105 °C deposition temperature, the radius of curvature increases with increasing film thickness when the film thickness is greater than 74 nm. The surface roughness (R_a) of the uncoated SiN_x is 1.35 ± 0.06 nm, and the roughness after Al deposition is still in a good quality except for the one of the thickness of 364 nm deposited at room temperature. Using these deflections and the mechanical properties of Al and SiN_x listed in Table I,^{26,32,33} the residual stresses in microcantilevers are analyzed as follows.

Stoney's equation has been used extensively to characterize residual stresses in a thin film grown or deposited on a substrate, such that³⁴

$$\sigma_{st} = \frac{E_s h_s^2}{6(1 - \nu_s) h_f r} \quad (1)$$

where σ_{st} is the film stress (by Stoney's equation), E , ν and h are Young's modulus, Poisson's ratio, and thickness, respectively. The subscripts, s and f, denote the substrate and the film, respectively, and r is the radius of curvature of the bilayer system. Note that the curvature is positive when the film surface is concave. The term $E/(1 - \nu)$ denotes the biaxial modulus. However, it is worthwhile to point out that Stoney's equation is valid only when the film has a negligible thickness compared to the substrate.

When the film thickness is not negligible, Hsueh and Lee¹² proposed a method to solve the stress gradient through the thickness in an elastic bilayer arising from the bending

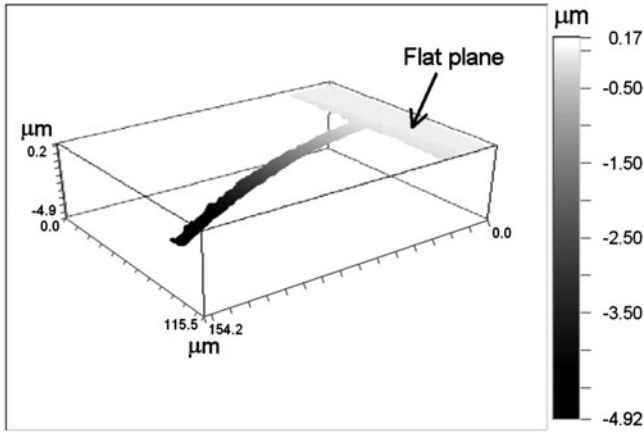
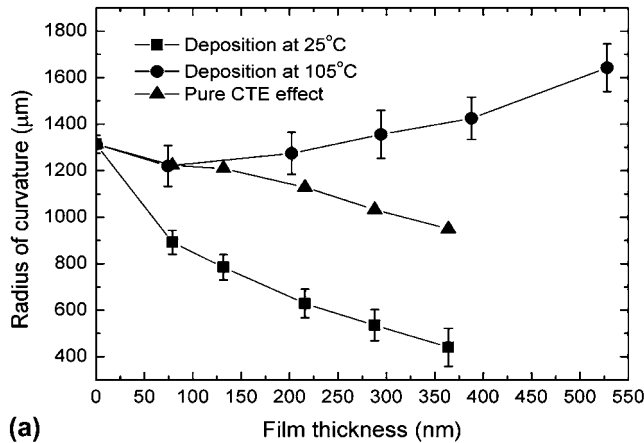
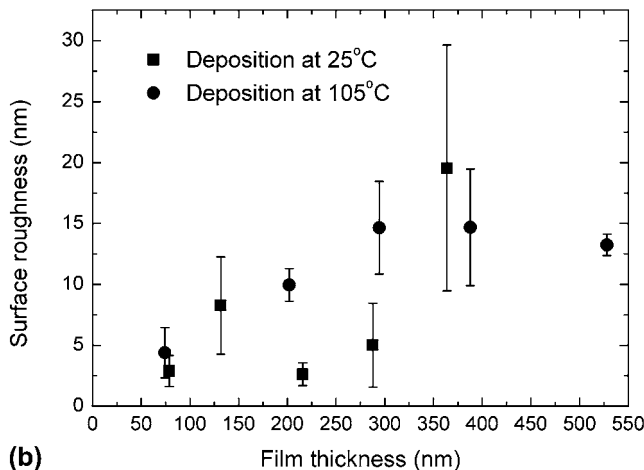


FIG. 2. An uncoated silicon nitride microcantilever measured by WYKO interferometer shows an intrinsic deflection. Note that the flat plane on the right-hand side is the surface of the silicon nitride film on the silicon wafer.



(a)



(b)

FIG. 3. (a) Radius of curvature of microcantilever and (b) surface roughness of the Al films as functions of Al film thickness.

curvature. The stresses in the substrate, σ_s , and in the film, σ_f , are

$$\sigma_s = B_s \varepsilon \text{ for } -h_s \leq z \leq 0 \quad , \quad (2a)$$

$$\sigma_f = B_f (\varepsilon - \Delta \varepsilon_f) \text{ for } -0 \leq z \leq h_f \quad . \quad (2b)$$

Note that B is the biaxial modulus and $\Delta \varepsilon$ is the unconstrained differential strain of the film with respect to the substrate. The total strain, ε , can be decomposed into the uniform strain c and the bending strain components, such that

$$\varepsilon = c + \frac{z - t_b}{r} \quad , \quad (3)$$

where z is the coordinate axis normal to film/substrate plane, the interface between the film and the substrate is located at $z = 0$ as shown in Fig. 4, and $z = t_b$ is the location of the bending axis corresponding to zero bending strain. Note that the second term on the right-hand side of Eq. (3) denotes the bending strain component. The solutions subjected to the force equilibrium and moment equilibrium conditions are

$$c = \frac{B_f h_f \Delta \varepsilon}{B_f h_f + B_s h_s} \quad , \quad (4)$$

$$t_b = \frac{B_f h_f^2 - B_s h_s^2}{2(B_f h_f + B_s h_s)} \quad , \quad (5)$$

TABLE I. Mechanical and thermal properties of Al and silicon nitride.

Materials	Young's modulus (GPa)	Poisson's ratio	Coefficient of thermal expansion ($10^{-6} \text{ } ^\circ\text{C}^{-1}$)
Al	70.0	0.35	23.1
SiN _x	260.5	0.29	3.3

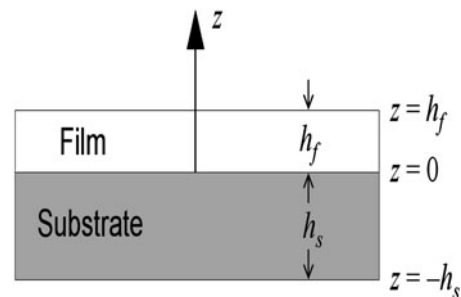


FIG. 4. Schematics showing the cross section of a film/substrate system in modeling.

$$\frac{1}{r} = \frac{6B_f B_s h_f h_s (h_f + h_s) \Delta \varepsilon}{B_f^2 h_f^4 + B_s^2 h_s^4 + 2B_f B_s h_f h_s (2h_f^2 + 2h_s^2 + 3h_f h_s)} \quad (6)$$

Equation (6) can be used to calculate the differential strain if the radius of curvature, biaxial modulus, and thicknesses of films and substrates are given. Note that the curvature is positive when the film surface is convex for the present solution. Thus, the sign of curvature in the present solution is opposite to that in Stoney's equation (e.g., the curvature shown in Fig. 2 is positive). The average film stress is defined by

$$\bar{\sigma}_f = \frac{1}{h_f} \int_0^{h_f} \sigma_f dz \quad (7)$$

Using Eqs. (3)–(6) and substituting Eq. (2b) into Eq. (7), the average film stress is

$$\bar{\sigma}_f = \frac{-B_f B_s h_s (B_f h_f^3 + B_s h_s^3) \Delta \varepsilon}{B_f^2 h_f^4 + B_s^2 h_s^4 + 2B_f B_s h_f h_s (2h_f^2 + 2h_s^2 + 3h_f h_s)} \quad (8)$$

Considering the presence of curvature of the cantilever before film deposition, the effective curvature $1/r$ induced by the film deposition process and the mismatch between the film and the substrate is

$$1/r = 1/r_A - 1/r_B \quad (9)$$

where $1/r_A$ and $1/r_B$ are the curvatures of microcantilever after and before film deposition, respectively. This effective curvature is used in Eqs. (1) and (6) to calculate the residual stresses. From the data shown in Fig. 3(a), the (effective) curvature $1/r$ is obtained. Then the differential strain $\Delta \varepsilon$ and total strain ε can be obtained from Eqs. (6) and (3), respectively. Using Eq. (2), the stress distributions in the Al film and SiN_x substrate at 25 and 105 °C are shown in Figs. 5(a) and 5(b), respectively. For the Al film deposited at 25 °C, the stress in the Al film is always compressive regardless of the film thickness as shown in Fig. 5(a) and its magnitude at the free surface of the film is smaller than that at the film/substrate interface.

Because thermal mismatch is excluded at room temperature deposition, the stresses in microcantilever originate from other sources such as dislocations or interfaces, etc. The stress in the SiN_x substrate is (in-plane) compressive near the bottom free surface and tensile near the interface. However, for the Al film deposited at 105 °C, the stress in the Al film changes from compressive to tensile as the Al film thickness is greater than 294.4 nm [see Fig. 5(b)]. The stress state in the SiN_x substrate also changes at the 294.4 nm film thickness.

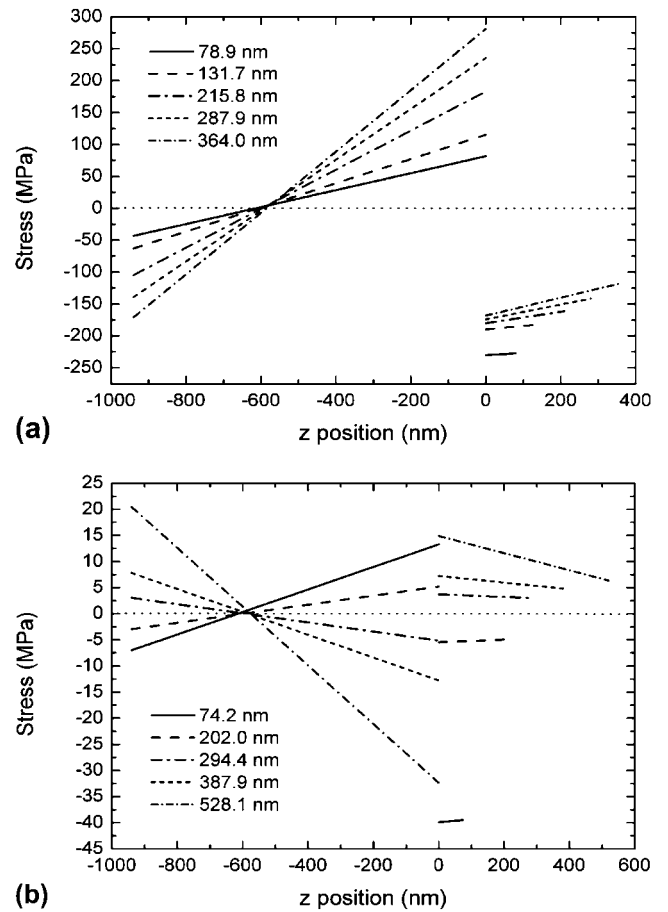


FIG. 5. Stress distributions in substrates and Al films evaporated at (a) room temperature and (b) 105 °C.

Such a change is due to the thermal mismatch between Al and SiN_x and other sources. As seen in Table I, the coefficient of thermal expansion (CTE) of Al is larger than the CTE of SiN_x . For pure thermal mismatch by cooling from 105 to 25 °C ($\Delta T = -80^\circ\text{C}$), the curvature induced by thermal mismatch can be calculated using Eq. (6) with $\Delta \varepsilon$ replaced by $(\alpha_f - \alpha_s) \Delta T$, such that^{1,13,14}

$$\frac{1}{r} = \frac{6B_f B_s h_f h_s (h_f + h_s) (\alpha_f - \alpha_s) \Delta T}{B_f^2 h_f^4 + B_s^2 h_s^4 + 2B_f B_s h_f h_s (2h_f^2 + 2h_s^2 + 3h_f h_s)} \quad (10)$$

where α is the CTE. It is assumed in this study that other than the difference in thermal mismatch, the two systems deposited at room temperature and 105 °C have the same sources to produce the residual stresses. In this case, the curvature of the system with Al deposited at 105 °C can be obtained from that with Al deposited at 25 °C by simply adding the curvature induced by the thermal mismatch with $\Delta T = -80^\circ\text{C}$. That is, the curvature shown by \blacktriangle is the summation of curvatures shown by \blacksquare and induced by the thermal mismatch. The symbols \bullet and \blacksquare stand for the experimental data of Al deposited at 105 and 25 °C,

respectively. Comparing the values for symbols \blacktriangle and \bullet , the difference of radius of curvature increases with the film thickness. This is contradicting to the above assumption. It implies that the defects to produce the residual stresses in the system deposited at room temperature are different from those at 105 °C. The microstructures of microcantilever deposited at 25 and 105 °C will be studied in the near future.

Using Eqs. (1) and (8), the average film stresses calculated from our experimental results are shown in Tables II and III. The average film stresses calculated by Stoney's equation are always higher than the values calculated by the present solution regardless of the deposition temperature and film thickness. In addition, the thicker the film, the larger the difference is. For a thick film, the Stoney's equation was corrected by the factor $(1 + \gamma\delta^3)/(1 + \delta)$, where γ designates the ratio of film

TABLE II. The average residual stresses $\bar{\sigma}_f$ and σ_{Sr} (by Stoney) in Al film deposited at 25 °C.

h_f (nm)	h_f/h_s	$\bar{\sigma}_f$ (MPa)	σ_{Sr} (MPa)
78.9	0.08	-228.93	-248.12
131.7	0.14	-186.23	-212.09
215.8	0.23	-170.77	-208.92
287.9	0.31	-157.84	-203.87
364.0	0.39	-142.93	-194.59

TABLE III. The average residual stress $\bar{\sigma}_f$ and σ_{Sr} (by Stoney) in Al film deposited at 105 °C.

h_f (nm)	h_f/h_s	$\bar{\sigma}_f$ (MPa)	σ_{Sr} (MPa)
74.2	0.08	-39.69	-42.83
202.0	0.21	-5.22	-6.32
294.4	0.31	3.37	4.38
387.9	0.41	6.03	8.31
528.1	0.56	10.62	15.67

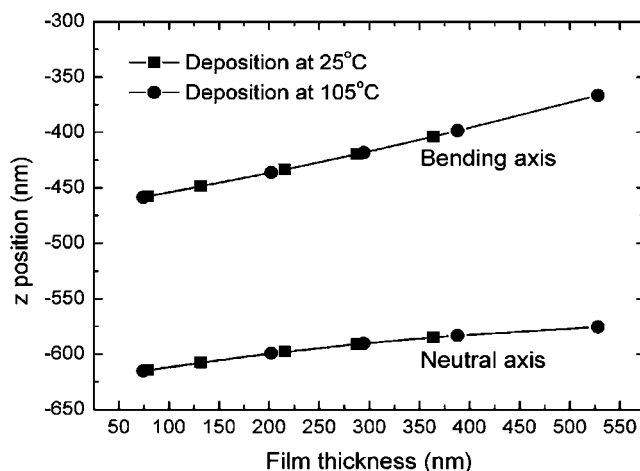


FIG. 6. Bending axis and neutral axis as functions of Al film thickness.

biaxial modulus to substrate biaxial modulus and δ is the ratio of film thickness to substrate thickness.^{1,35} In this study, the correction factor is in the range from 0.92 to 0.67 for δ from 0.08 to 0.56. The results of Stoney's equation after correction are the same as the values obtained from the present solution. The neutral axes and bending axes after Al deposition with different thicknesses are shown in Fig. 6. Both neutral axes and bending axes are located in the substrate and shift slightly toward the interface between Al film and SiN_x substrate when the film thickness is increased. Note that there is no temperature effect on either neutral axes or bending axes because they are influenced by geometry, materials properties, and plastic deformation.

IV. CONCLUSIONS

The residual stresses in the Al/ SiN_x system measured by the microcantilever were investigated. Various thicknesses of Al films were deposited on SiN_x microcantilevers by evaporation at 25 and 105 °C. For the room-temperature-deposited microcantilevers, the residual stress in the Al film was compressive and the microcantilever deflected toward the side of SiN_x substrate. For the Al film deposited at 105 °C and when the thickness ratio of film to substrate was greater than 0.31, the residual stress in the Al film became tensile and the microcantilever deflected toward the side of Al film. The average film stresses calculated by Stoney's equation were greater than those calculated by the present solution regardless of the deposition temperature and film thickness. Using the correction factor of $(1 + \gamma\delta^3)/(1 + \delta)$, the results of Stoney's equation become the same as those obtained from the present solution. Both neutral axes and bending axes are located in the substrate and their positions vary with the film thickness, but they are independent of deposition temperature.

ACKNOWLEDGMENT

This work was performed under the auspices of the National Science Council, Taiwan.

REFERENCES

- C.H. Hsueh: Modeling of elastic deformation of multilayers due to residual stresses and external bending. *J. Appl. Phys.* **91**, 9652 (2002).
- W. Fang and C.-Y. Lo: On the thermal expansion coefficients of thin films. *Sens. Actuators, A* **84**, 310 (2000).
- W. Fang and J.A. Wickert: Determining mean and gradient residual stresses in thin films using micromachined cantilevers. *J. Micromech. Microeng.* **6**, 301 (1996).
- S.G. Mayr and K. Samwer: Model for intrinsic stress formation in amorphous thin films. *Phys. Rev. Lett.* **87**, 036105 (2001).
- R. Koch: The intrinsic stress of polycrystalline and epitaxial thin metal films. *J. Phys. Condens. Matter* **6**, 9519 (1994).

6. W.D. Nix and B.M. Clemens: Crystallite coalescence: A mechanism for intrinsic tensile stresses in thin films. *J. Mater. Res.* **14**, 3467 (1999).
7. T.-Y. Zhang, S. Lee, L.J. Guido, and C.H. Hsueh: Criteria for formation of interface dislocations in a finite thickness epilayer deposited on a substrate. *J. Appl. Phys.* **85**, 7579 (1999).
8. R.C. Cammarata and T.M. Trimble: Surface stress model for intrinsic stresses in thin films. *J. Mater. Res.* **15**, 2468 (2000).
9. M. Pletea, R. Koch, H. Wendrock, R. Kaltofen, and O.G. Schmidt: *In situ* stress evolution during and after sputter deposition of Al thin films. *J. Phys. Condens. Matter* **21**, 1 (2009).
10. S.P. Kim, H.M. Choi, and S.K. Choi: A study on the crystallographic orientation with residual stress and electrical property of Al films deposited by sputtering. *Thin Solid Films* **322**, 298 (1998).
11. J.H. Lee, W.M. Kim, T.S. Lee, M.K. Chung, B.K. Cheong, and S.G. Kim: Mechanical and adhesion properties of Al/AlN multilayered thin films. *Surf. Coat. Tech.* **133-134**, 220 (2000).
12. C.H. Hsueh and S. Lee: Effects of viscous flow on residual stresses in film/substrate systems. *J. Appl. Phys.* **91**, 2760 (2002).
13. Y.Y. Hu and W.M. Huang: Elastic and elastic-plastic analysis of multilayer thin films: Closed-form solutions. *J. Appl. Phys.* **96**, 4154 (2004).
14. C.H. Hsueh, S. Lee, and H.-Y. Lin: Analyses of mode I edge delamination by thermal stresses in multilayer systems. *Compos. Eng.* **37**, 1 (2006).
15. J.C. Tsang, P.M. Mooney, F. Dacol, and J.O. Chu: Measurements of alloy composition and strain in thin $\text{Ge}_x\text{Si}_{1-x}$ layers. *J. Appl. Phys.* **75**, 8098 (1994).
16. T.S. Perova, K. Lyutovich, E. Kasper, A. Waldron, M. Oehme, and R.A. Moore: Stress determination in strained-Si grown on ultra-thin SiGe virtual substrates. *Mater. Sci. Eng., B* **135**, 192 (2006).
17. Y. Zoo, D. Adams, J.W. Mayer, and T.L. Alford: Investigation of coefficient of thermal expansion of silver thin film on different substrates using x-ray diffraction. *Thin Solid Films* **513**, 170 (2006).
18. W.D. Nix: Mechanical properties of thin films. *Metall. Trans. A* **20**, 2217 (1989).
19. W. Fang and J.A. Wickert: Comments on measuring thin-film stresses using bi-layer micromachined beams. *J. Micromech. Microeng.* **5**, 276 (1995).
20. W. Fang, H.-C. Tsai, and C.-Y. Lo: Determining thermal expansion coefficients of thin films using micromachined cantilevers. *Sens. Actuators, A* **77**, 21 (1999).
21. M.T.-K. Hou and R. Chen: Effect of width on the stress-induced bending of micromachined bilayer cantilevers. *J. Micromech. Microeng.* **13**, 141 (2003).
22. J. McCarthy, Z. Pei, M. Becker, and D. Atteridge: FIB micro-machined submicron thickness cantilevers for the study of thin film properties. *Thin Solid Films* **358**, 146 (2000).
23. F.L. Riley: Silicon nitride and related materials. *J. Am. Ceram. Soc.* **83**, 245 (2000).
24. S. Akamine, R.C. Barrett, and C.F. Quate: Improved atomic force microscope images using microcantilevers with sharp tips. *Appl. Phys. Lett.* **57**, 316 (1990).
25. R.J. Grow, S.C. Minne, S.R. Manalis, and C.F. Quate: Silicon nitride cantilevers with oxidation-sharpened silicon tips for atomic force microscopy. *J. Microelectromech. Syst.* **11**, 317 (2002).
26. A. Khan, J. Philip, and P. Hess: Young's modulus of silicon nitride used in scanning force microscope cantilevers. *J. Appl. Phys.* **95**, 1667 (2004).
27. M.B. Viani, T.E. Schäffer, A. Chand, M. Rief, H.E. Gaub, and P.K. Hansma: Small cantilevers for force spectroscopy of single molecules. *J. Appl. Phys.* **86**, 2258 (1999).
28. Y. Toivola, J. Thurn, R.F. Cook, G. Cibuzar, and K. Roberts: Influence of deposition conditions on mechanical properties of low-pressure chemical vapor deposited low-stress silicon nitride films. *J. Appl. Phys.* **94**, 6915 (2003).
29. S. Habermehl: Stress relaxation in Si-rich silicon nitride thin films. *J. Appl. Phys.* **83**, 4672 (1998).
30. W. Shi, H. Zhang, G. Zhang, and Z. Li: Modifying residual stress and stress gradient in LPCVD Si_3N_4 film with ion implantation. *Sens. Actuators, A* **130-131**, 352 (2006).
31. H. Bouridah, F. Mansour, M.R. Beghou, R. Mahamdi, and P. Temple-Boyer: Properties of non-stoichiometric nitrogen doped LPCVD silicon thin films. *Cryst. Res. Technol.* **45**, 119 (2010).
32. W.-H. Chuang, T. Luger, R.K. Fetting, and R. Ghodssi: Mechanical property characterization of LPCVD silicon nitride thin films at cryogenic temperatures. *J. Microelectromech. Syst.* **13**, 870 (2004).
33. C.-K. Huang, W.-M. Lou, C.-J. Tsai, T.-C. Wu, and H.-Y. Lin: Mechanical properties of polymer thin film measured by the bulge test. *Thin Solid Films* **515**, 7222 (2007).
34. G.G. Stoney: The tension of metallic films deposited by electrolysis. *Proc. R Soc. Lond., Ser. A* **82**, 172 (1909).
35. C.A. Klein: How accurate are Stoney's equation and recent modifications. *J. Appl. Phys.* **88**, 5487 (2000).